Nonlinear wind-tunnel wall-interference corrections using data assimilation

Belligoli, Zeno; Dwight, Richard P.; Eitelberg, Georg

DOI
10.2514/1.J059558

Publication date
2021

Document Version
Final published version

Published in
AIAA Journal

AIAA JOURNAL
Vol. 59, No. 2, February 2021

Nonlinear Wind-Tunnel Wall-Interference Corrections Using Data Assimilation

Zeno Belligoli,* Richard P. Dwight,† and Georg Eitelberg‡
Delft University of Technology, 2629 HS Delft, The Netherlands

https://doi.org/10.2514/1.J059558

This paper presents a novel approach for correcting wind-tunnel wall interference in the nonlinear flow regime, that is, in the presence of phenomena such as flow separation and shocks. The methodology uses a gradient-based optimization to minimize the difference between experimental measurements and a Favre-averaged Navier–Stokes (FANS) simulation. The aim is to exploit the high-fidelity experimental data to correct turbulence-modeling errors in the FANS simulations, as well as to use the accurate angle of attack and Mach number from the FANS simulations to correct the in-tunnel flow conditions. The optimization is carried out directly in free air, thus avoiding the requirement to mesh the wind-tunnel walls and/or to model the ventilated-wall boundary condition. A byproduct of this method is the availability of flow information everywhere around the test object, which augments and complements the experimental data. The methodology is tested on two-dimensional and three-dimensional flow cases, demonstrating a significant improvement in the agreement between experimental and numerical data.

Nomenclature

$\mathcal{B}(\cdot)$	=	projection operator
c	=	chord length, m
c_L	=	lift coefficient
c_p	=	pressure coefficient
$\boldsymbol{d}$	=	vector of observations
E	=	total energy per unit mass, m^2/s^2
E	=	total enthalpy per unit mass, m^2/s^2
$\boldsymbol{F}^c$	=	convective fluxes
$\boldsymbol{F}^v$	=	viscous fluxes, $kg/(m^2 \cdot s)$
$\mathcal{J}$	=	cost function
$\hat{\mathcal{J}}$	=	error function
k	=	turbulent kinetic energy, m^2/s^2
M_∞	=	freestream Mach number
N_d	=	number of observations
N_m	=	number of control variables
Pr	=	Prandtl number
R	=	ideal gas constant, $(kg \cdot m^2)/(K \cdot mol \cdot s^2)$
$\boldsymbol{R}$	=	Reynolds-stress tensor, m^2/s^2
$\mathcal{R}(\cdot)$	=	operator representing the Favre-averaged Navier–Stokes equations
$\boldsymbol{U}$	=	vector of state variables
$\boldsymbol{v}$	=	velocity vector, m/s
y^+	=	dimensionless wall distance
α_∞	=	freestream angle of attack, deg
$\boldsymbol{\beta}$	=	corrective term for the turbulence production
γ	=	ratio of specific heats
δ_{ij}	=	Kronecker delta
$\boldsymbol{\varepsilon}$	=	observation noise
$\boldsymbol{\theta}$	=	vector of control parameters
κ_T	=	thermal conductivity, $W/(m \cdot K)$
μ_{turb}	=	dynamic eddy viscosity, m^2/s
ρ	=	density, kg/m^3
σ_{exp}	=	observation standard deviation
σ_θ	=	control variable standard deviation
ω	=	specific dissipation rate, s^{-1}

Presented as Paper 2019-0939 at the AIAA Scitech 2019 Forum, San Diego, CA, January 7–11, 2019; received 29 February 2020; revision received 10 July 2020; accepted for publication 27 August 2020; published online 18 December 2020.

*Ph.D. Candidate, Department of Aerodynamics; z.belligoli@tudelft.nl.
†Associate Professor, Department of Aerodynamics; r.p.dwight@tudelft.nl.
‡Full Professor, Department of Aerodynamics.

I. Introduction

THE design of an air vehicle depends on techniques to assess performance in free air. These can either be experimental fluid dynamics (EFD) or computational fluid dynamics (CFD) techniques. Normally, EFD involves an experiment in a wind tunnel, and it has been the dominant tool for testing aeronautic designs for the majority of the 20th century. However, due to increases in computational speed and accuracy, there has been a steady decline in the wind-tunnel testing time relative to the CFD testing time [1]. Currently, CFD and EFD coexist, with the latter being used to test the design in the most challenging regions of the flight envelope, where uncertainties due approximations in the CFD models become substantial.

However, wind-tunnel experiments themselves have uncertainties. One of the most critical is due to the presence of the wind-tunnel walls, which alter the flowfield around the test object, making it different from what it would be in free air. The existence of a free-air flow giving the same forces and moments as those measured in the tunnel is the fundamental assumption of the entire practice of wind-tunnel corrections [2]. In presence of subsonic flow conditions, small angles of attack, and small cross section of the test object relative to that of the wind tunnel, then corrections can be based on linearized, inviscid potential flow theory, hence the name *linear corrections*. When one of these conditions is not satisfied, significant errors result. Despite these considerations, the majority of wind-tunnel operators still make use of linear corrections in the nonlinear regime or do not correct the data at all when nonlinear effects become too strong [3].

Several techniques have been proposed for nonlinear wind-tunnel wall-interference corrections. One of the most popular consists of taking the difference between a turbulent CFD simulation of the test object in the wind tunnel and in free flight [4–7] as well as using this information to adjust the experimental Mach number, the angle of attack, and (in some cases) force coefficients. The main challenges of this approach are the need to accurately model the geometry of the wind tunnel, the boundary conditions at ventilated walls [2,8], and the effect of turbulence. The first problem can be solved by using a detailed CAD file of the wind-tunnel geometry, although meshing such a domain is a time-consuming little-automated activity that produces an extremely large number of cells, thus significantly increasing the computational cost of the simulation. For the second problem, there exist many different formulations of the porous/ventilated-wall boundary condition, for which characterization of the crossflow at the wall remains problematic [9,10]. Finally, even if the first two problems were solved, modeling turbulent flow in the nonlinear regime is one of the most challenging tasks for the CFD

community because current turbulence models prove to be inaccurate in those conditions [11,12]. All these factors affect the quality of the wall-interference correction because, in essence, wall-interference correction techniques are strictly dependent on the computational infrastructure used to obtain them.

This study proposes a variational data assimilation (DA) approach combining experimental and numerical results in a systematic way, with the aim of simultaneously correcting for wind-tunnel wall interference and errors in the Favre-averaged Navier–Stokes (FANS) turbulence model, without needing to model the wind-tunnel geometry or the boundary conditions at the ventilated walls. The method minimizes the discrepancy between high-fidelity experimental observations and the numerical prediction of those same quantities by modifying the freestream Mach number, angle of attack, and a local corrective term for the turbulence model. In this way, experimental data are used to correct the CFD simulations and, in turn, the CFD simulations are used to correct the Mach number and angle of attack of the experiments, thus returning the free-air conditions corresponding to the in-tunnel flowfield. The numerical optimization is carried out directly in free air, thus simplifying the meshing process and reducing the total number of mesh points thanks to the absence of the wind-tunnel walls.

To our knowledge, only a few studies have addressed the problem of wind-tunnel interference corrections by means of data assimilation. The idea of injecting experimental data into computer simulations for correcting wall interference was first introduced by Murman [13], who proposed to minimize the difference between the experimental and numerical pressures on a supercritical airfoil by using the freestream Mach number and angle of attack as control parameters. This approach was tested with success on synthetic data but did not take into account the influence of viscosity in a comprehensive manner. Only recently, Ma et al. [14] extended it to a viscous code using a variational data assimilation procedure on two-dimensional (2-D) airfoils in the transonic regime. Their results showed that the methodology was able to not only to obtain pressure contours that closely matched the experimental ones, but it was also able to obtain accurate estimations of the lift and pitching-moment coefficients. However, they did not take into account the errors associated with the choice of turbulence model, which could yield misleading results for the corrected angle of attack and Mach number, especially in strongly nonlinear conditions. This problem was acknowledged by Kato et al. [15], who proposed a DA framework based on the ensemble Kalman filter with the capability to estimate not only the angle of attack and Mach number but also other parameters influencing the turbulence model, such as the von Kármán constant. By doing this, they were able to address the uncertainty associated with the values of (one of) the closure coefficients of the turbulence model, thus providing insights into the variability of the model outputs. Nevertheless, this technique is limited in scope since the functional form of the turbulence model is frozen, thus preventing corrections to the balance of terms within the turbulence model, which is an important factor for the accurate prediction of turbulent flows [16].

Having acknowledged this, Singh and Duraisamy [16], Duraisamy et al. [17], Parish and Duraisamy [18], and Singh et al. [19] recently developed a variational data assimilation framework for the correction of FANS turbulence-model errors using a corrective scalar field as a multiplicative factor to the production term in the turbulence model.

In its essence, the methodology proposed in this work combines the ideas of Murman [13] and Ma et al. [14] with the seminal work of Singh and Duraisamy [16], Duraisamy et al. [17], Parish and Duraisamy [18], and Singh et al. [19] to build a variational data assimilation technique capable of correcting the experimental angle of attack and Mach number, as well as the model form errors in the turbulence model. In our previous work [20,21], we carried out a preliminary study showing the potential of this idea. Here, we formally derive the expression of the objective function from a probabilistic point of view (Sec. II); we apply the methodology to both 2-D and three-dimensional (3-D) cases, and we compare it to linear correction methods (Sec. III). Furthermore, we discuss the capabilities of the DA framework to correctly infer unobserved quantities such as the velocity field around the test object or the volumetric pressure field. Finally, we summarize the main conclusions and propose further developments in Sec. IV.

II. Methodology

This section lays the foundations of the data assimilation methodology for correcting nonlinear wind-tunnel wall interference. Strong nonlinear flow effects can only be described by a nonlinear model. Because nonlinearities are often associated with transonic conditions, we choose the Favre-averaged Navier–Stokes equations as our nonlinear model (this is the standard choice for numerical simulations of compressible flows). If a sufficiently refined CAD model and mesh are used, as well as adequate thresholds for the convergence of iterative numerical methods, the largest source of error in a FANS code is due to the turbulence model [11,12]. In principle, if this error was removed, the FANS equations would be able to exactly predict the mean flow, and wind-tunnel experiments would become almost redundant.

In practice, the present work uses experimental data to correct turbulence-modeling errors, thus connecting CFD and EFD to obtain accurate and additional information about the flow configuration under study. To do so, we propose a variational data assimilation framework that uses a gradient-based algorithm to optimize the values of the freestream angle of attack, Mach number, and a corrective term of the turbulence model by minimizing the difference between sparse experimental observations and their numerical prediction with a FANS code.

This is an ill-posed inverse problem for which the solution is nonunique. Hence, while it is theoretically possible to reconstruct the true flowfield, in practice, this seldom happens; and the numerical flowfield is somewhat different from the true one. The optimization problem is

$$\begin{aligned} \min_{\boldsymbol{\theta}} \quad & \mathcal{J} \\ \text{subject to} \quad & \mathcal{R}(\boldsymbol{U},\boldsymbol{\theta}) = 0 \end{aligned} \tag{1}$$

where $\mathcal{J} = \|\boldsymbol{d}_{\mathrm{CFD}}(\boldsymbol{\theta}) - \boldsymbol{d}_{\mathrm{EXP}}\|_p + \|\boldsymbol{\theta}\|_p$; $\|\cdot\|_p$ is the L_p norm; $\boldsymbol{d}_{\mathrm{EXP}}$ and $\boldsymbol{d}_{\mathrm{CFD}}$ are the experimental and numerical observations, respectively; $\boldsymbol{\theta}$ is the high-dimensional vector of control parameters; and $\mathcal{R}$ is the operator representing the FANS equations, the turbulence model, and their boundary conditions. The first term in $\mathcal{J}$ is the difference between experimental and numerical quantities in a certain norm, whereas the second is a regularization term that selects one particular solution form the large space of possible ones.

Gradient-based methods are suited for this type of high-dimensional optimization thanks to the adjoint approach [22,23]: a mathematical technique that allows one to obtain the gradients of the objective function with respect to *any* number of control parameters at the cost of only one additional flow evaluation [24,25]. Thanks to the work of Albring et al. [26,27], the SU2 [28,29] CFD software comes with a discrete adjoint framework based on algorithmic differentiation that makes it possible to obtain the gradients of many objective functions with minimal source code modifications.

This work makes use of the low-memory Broyden–Fletcher–Goldfarb–Shanno [30] optimization algorithm to update the value of the control parameters and compute the step size of the optimization. The initial angle of attack and Mach number can be specified to be the in-tunnel ones, whereas the initial corrective term can be specified in such a way that the result of the first optimization iteration is that of a FANS simulation with an uncorrected turbulence model. Finally, the optimization terminates when either

$$\max(|\partial_i \mathcal{J}|) \leq 5 \cdot 10^{-5} \quad \text{for } i = 1, \ldots, N_m$$

or

$$\frac{\mathcal{J}^q - \mathcal{J}^{q+1}}{\max\{|\mathcal{J}^q|, |\mathcal{J}^{q+1}|, 1\}} \leq 10^{-3}$$

where q is the qth optimization iteration, $\partial_i \mathcal{J}$ is the gradient of the objective function with respect to the ith control parameter, N_m is the number of control parameters, and the value of the thresholds are specified by the user.

The optimum solution gives the best agreement between the experimental and numerical quantities, and it directly provides the corrected values of the freestream angle of attack and Mach number while also minimizing the error due to the approximation of the Reynolds-stress tensor by the turbulence model. It is worth noting that this method can work with any kind of experimental data; for example, $\boldsymbol{d}_{\mathrm{EXP}}$ may be a 3-D velocity field from particle image velocimetry, or pressure on a surface, or a combination of both.

The drawback of this methodology is that the optimization procedure is computationally time consuming, especially in three dimensions or in the presence of complicated flow cases, and therefore can only be performed offline at the end of the experimental campaign. This may not be ideal when the correctability of the data has to be assessed during an experiment. In that case, simpler but faster techniques should be used. In addition, nonuniqueness of the solution and convergence to local minima tend to make the final corrections suboptimal. Although these problems influence the accuracy of the corrections, and of the reconstructed flowfield, in practice, their effect is limited, provided the objective function is regularized and the initial value of the vector of control parameters is in a neighborhood of the true optimum.

In the following sections, the FANS equations (Sec. II.A) and the Bayesian derivation of the objective function (Sec. II.B) are presented.

A. FANS Equations

The compressible Navier–Stokes equations with no source term or domain motion are

$$\partial_t \boldsymbol{U} + \nabla \cdot \boldsymbol{F}^c - \nabla \cdot \boldsymbol{F}^v = \boldsymbol{0} \quad \text{in } \Omega, t > 0 \tag{2}$$

where $\Omega \subset \mathbb{R}^3$ is the fluid domain, $\boldsymbol{U} = [\rho, \rho v_1, \rho v_2, \rho v_3, \rho E]^\top$ is the vector of conservative variables, ρ is the fluid density, E is the total energy per unit mass, and $\boldsymbol{v} = [v_1, v_2, v_3]^\top \in \mathbb{R}^3$ is the flow velocity in a Cartesian coordinate system. $\boldsymbol{F}^c$ and $\boldsymbol{F}^v$ are the convective and viscous fluxes, which can be written as

$$\boldsymbol{F}_i^c = \begin{pmatrix} \rho v_i \\ \rho v_i v_1 + p\delta_{i1} \\ \rho v_i v_2 + p\delta_{i2} \\ \rho v_i v_3 + p\delta_{i3} \\ \rho v_i H \end{pmatrix}, \quad \boldsymbol{F}_i^v = \begin{pmatrix} \cdot \\ \tau_{i1} \\ \tau_{i2} \\ \tau_{i3} \\ v_j \tau_{ij} + k_T \partial_i T \end{pmatrix}, \quad i = 1,\ldots,3 \tag{3}$$

where p is the static pressure; T is the temperature; $H = h + v_i v_i/2 = E + p/\rho$ is the total enthalpy; δ_{ij} is the Kronecker delta; and κ_T is the thermal conductivity for a calorically perfect fluid. The viscous stresses are of molecular origin and can be compactly written as

$$\tau_{ij} = \mu\left(\partial_j v_i + \partial_i v_j - \frac{2}{3}\partial_n v_n \delta_{ij}\right) = \mu\left(2S_{ij} - \frac{2}{3}\partial_n v_n \delta_{ij}\right) \tag{4}$$

Assuming the fluid is a perfect gas with a ratio of specific heats $\gamma = (c_p/c_v)$ and a gas constant R, the pressure is determined from

$$p = (\gamma - 1)\rho\left[E - \frac{1}{2}(\boldsymbol{v} \cdot \boldsymbol{v})\right] \tag{5}$$

and the temperature is given by

$$T = \frac{p}{\rho R} \tag{6}$$

When working with compressible flows, a density-weighted (or Favre) averaging is used, with $\tilde{A} = \overline{\rho A}/\bar{\rho}$ being the Favre-averaged mean quantity, with A'' representing the turbulent fluctuations such that an instantaneous flow variable can be written as $A = \tilde{A} + A''$; and $\bar{(\cdot)}$ is the notation for Reynolds-averaged mean quantities. The application of Favre averaging to the Navier–Stokes equations returns the compressible Reynolds-averaged Navier–Stokes equations, which are also known as Favre-averaged Navier–Stokes equations. The FANS equations can be written as

$$\partial_t \begin{pmatrix} \bar{\rho} \\ \bar{\rho}\tilde{v}_1 \\ \bar{\rho}\tilde{v}_2 \\ \bar{\rho}\tilde{v}_3 \end{pmatrix} + \nabla \cdot \begin{pmatrix} \bar{\rho}\tilde{v}_i \\ \bar{\rho}\tilde{v}_i\tilde{v}_1 + \bar{p}\delta_{i1} \\ \bar{\rho}\tilde{v}_i\tilde{v}_2 + \bar{p}\delta_{i2} \\ \bar{\rho}\tilde{v}_i\tilde{v}_3 + \bar{p}\delta_{i3} \\ \bar{\rho}\tilde{v}_i\tilde{H} \end{pmatrix} - \nabla \cdot \begin{pmatrix} \cdot \\ \tilde{\tau}_{i1} - \overline{\rho v_i'' v_1''} \\ \tilde{\tau}_{i2} - \overline{\rho v_i'' v_2''} \\ \tilde{\tau}_{i3} - \overline{\rho v_i'' v_3''} \\ \tilde{v}_j\tilde{\tau}_{ij} + \kappa_T \partial_i \tilde{T} + \overline{\rho v_j'' h''} - \tilde{v}_j \overline{\rho v_i'' v_j''} \end{pmatrix} = \boldsymbol{0} \tag{7}$$

Aside from replacement of instantaneous variables by mean values, the only difference between the Favre-averaged and instantaneous momentum equations is the appearance of the correlation $-\overline{\rho v_i'' v_j''}$, which can also be written as $-\bar{\rho}\,\widetilde{v_i'' v_j''}$ [31]. The mean energy equation presents $-\overline{\rho v_i'' v_j''}$ as well as a turbulent heat flux $\overline{\rho v_j'' h''}$ in addition to the terms of the instantaneous formulation.

The component $\widetilde{v_i'' v_j''}$ is a symmetric positive-definite tensor commonly referred to as the Reynolds-stress tensor (RST). To study the effect of turbulence on the mean flow, the Reynolds-stress tensor can be decomposed into an anisotropic part and an isotropic part:

$$R_{ij} = \widetilde{v_i'' v_j''} = 2k\left(b_{ij} + \frac{\delta_{ij}}{3}\right) \tag{8}$$

where $k = \widetilde{v_i'' v_i''}/2$ is the turbulent kinetic energy, $2kb_{ij} = a_{ij}$ is the anisotropy tensor, and $(2k/3)\delta_{ij}$ is the isotropic part of the RST. The relations between the components of the Reynolds-stress tensor and the mean flow quantities are unknown. Therefore, in order to close the system of equations, a model for these unknown relations must be introduced. Linear eddy viscosity models (EVMs) are the most widespread in industry. They are based on the Boussinesq approximation, which reduces the effect of the anisotropic part of the Reynolds stresses to only an added viscosity such that

$$\widetilde{v_i'' v_j''} - \frac{2}{3}k\delta_{ij} \approx -\frac{\mu_{\mathrm{turb}}}{\rho}\left(\partial_j \tilde{v}_i + \partial_i \tilde{v}_j - \frac{2}{3}\delta_{ij}\nabla \cdot \tilde{\boldsymbol{v}}\right) \tag{9}$$

where μ_{turb} is the turbulent (or eddy) viscosity. The Boussinesq approximation assumes the anisotropic part of the Reynolds-stress tensor is proportional to the mean strain rate tensor $\tilde{S}_{ij} = (1/2)(\partial_j \tilde{v}_i + \partial_i \tilde{v}_j)$, leaving the turbulent viscosity as the only unknown. Linear EVMs introduce additional transport equations for quantities connected to μ_{turb} in order to obtain a closed system of equations. Finally, the turbulent heat-flux vector $\overline{\rho v_j'' h''}$ is approximated as

$$\overline{\rho v_j'' h''} = -\frac{\mu_{\mathrm{turb}} c_p}{Pr_{\mathrm{turb}}}\frac{\partial \tilde{T}}{\partial x_j} = -\frac{\mu_{\mathrm{turb}}}{Pr_{\mathrm{turb}}}\frac{\partial \tilde{h}}{\partial x_j} \tag{10}$$

where Pr_{turb} is the turbulent Prandtl number, which is usually assumed to be 0.90.

When errors due to the level of discretization of the computational mesh or the iterative convergence of the algorithms are minimized, the modeling of the Reynolds-stress tensor becomes the major source of uncertainty in a CFD simulation; and it is the reason why wind-tunnel experiments are still required. In this work, we focus on Menter's shear-stress transport (SST) [32] turbulence model, but similar considerations hold for all linear EVMs. The SST model has two transport equations: one for the turbulent kinetic energy k, and one for the specific dissipation rate ω. Its general structure is

$$\frac{Dk}{Dt} = P_k(k,\omega,\boldsymbol{U}) - D_k(k,\omega,\boldsymbol{U}) + T_k(k,\omega,\boldsymbol{U}) \tag{11}$$

$$\frac{D\omega}{Dt} = P_\omega(k,\omega,\boldsymbol{U}) - D_\omega(k,\omega,\boldsymbol{U}) + T_\omega(k,\omega,\boldsymbol{U}) \tag{12}$$

where $P(\cdot)$, $D(\cdot)$, and $T(\cdot)$ are the production, destruction, and cross-production terms, respectively. Following Singh and Duraisamy [16] and Parish and Duraisamy [18], a multiplicative corrective term can be introduced into the turbulence model in order to correct the functional form of the model discrepancy. This could be easily achieved by rewriting the production term in one of the transport equations as $\beta(\boldsymbol{x}) \cdot P(\cdot)$. Like $P(\cdot)$, β is a spatially varying scalar field defined everywhere in the domain. The corrective term can take values both larger and smaller than unity, thus being able to influence the balance of terms in the transport equation and, in turn, the mean solution of the FANS equations. After the discretization of the FANS equations, $\boldsymbol{\beta}$ is represented as a high-dimensional vector, with as many elements as the number of mesh points, and with the baseline model having an initial value of unity, i.e., $\boldsymbol{\beta} = \mathbf{1}$.

B. Bayesian Formulation of the Inverse Problem

Quantities $\boldsymbol{d} \in \mathbb{R}^{N_d}$ measured experimentally differ from the true values of those quantities $\boldsymbol{d}_{\text{true}} \in \mathbb{R}^{N_d}$ due to measurement noise and experimental bias. We model this discrepancy statistically as

$$\boldsymbol{d} = \boldsymbol{d}_{\text{true}} + \boldsymbol{\varepsilon}, \qquad \boldsymbol{\varepsilon} \sim \mathcal{N}(0, \sigma_{\text{exp}}^2) \tag{13}$$

where we assume zero bias, and we assume noise to be independent identically distributed (i.i.d.) normal random variables with known standard deviation σ_{exp} (obtained from the experimental procedure). Given some flow state $\boldsymbol{U} = [\rho, \rho\boldsymbol{v}, \rho E, \rho k, \rho\omega]^\top \in \mathcal{U}$, let $\mathcal{B}: \mathcal{U} \to \mathbb{R}^{N_d}$ be a projection that extracts the measured quantities. Under most circumstances (including here), this operator will have negligible error so that $\boldsymbol{d} = \mathcal{B}(\boldsymbol{U}_{\text{true}}) + \boldsymbol{\varepsilon}$ is a reasonable generalization of Eq. (13) (where $\boldsymbol{U}_{\text{true}} \in \mathcal{U}$ is the true state). However, $\boldsymbol{U}_{\text{true}}$ is unknown, and it is approximated by solving the FANS equations including boundary conditions

$$\mathcal{R}(\hat{\boldsymbol{U}}) = 0 \tag{14}$$

where $\hat{\boldsymbol{U}} \neq \boldsymbol{U}_{\text{true}}$, introducing a nonnegligible modeling error. Following the seminal work of Kennedy and O'Hagan [33] and previous work in fluid dynamics [34,35], we could write

$$\boldsymbol{d} = \boldsymbol{\psi}(\boldsymbol{x}) \cdot \mathcal{B}(\hat{\boldsymbol{U}}) + \boldsymbol{\varepsilon} \tag{15}$$

where $\boldsymbol{\psi} \sim \mathcal{GP}(\mu_\psi, r_\psi)$ is a Gaussian process needed to account for the errors in $\mathcal{R}(\cdot)$. A function of the spatial location $\boldsymbol{x}$ (e.g., see Ref. [36]), its mean $\mu_\psi(\cdot)$, and covariance functions $r_\psi(\cdot,\cdot)$ must be identified from the data (under some priors). This formulation allows predictions of the quantity $\boldsymbol{d}$ at unmeasured locations, but it says nothing about other quantities. For example, if $\boldsymbol{d}$ are measurements of pressure, $\boldsymbol{\psi}$ represents the model error in pressure and does not speak to velocity.

Therefore, in this work, we deviate from Kennedy and O'Hagan's formulation [33] by moving the statistical term representing model error into the operator $\mathcal{R}$. This is logical: the source of error is within $\mathcal{R}$, and identification of this error will allow us to make predictions of unmeasured quantities. Let this discrepancy term be $\boldsymbol{\theta} \in \boldsymbol{\Theta}$, and modify the governing equations as

$$\mathcal{R}(\boldsymbol{U}, \boldsymbol{\theta}) = 0 \tag{16}$$

By the implicit function theorem, we can specify a function $\boldsymbol{U}: \boldsymbol{\Theta} \to \boldsymbol{\mathcal{U}}$ so that we can construct the statistical model

$$\boldsymbol{d} = \boldsymbol{d}_{\text{true}} + \boldsymbol{\varepsilon} = \mathcal{B}(\boldsymbol{U}(\boldsymbol{\theta})) + \boldsymbol{\varepsilon} \tag{17}$$

as an alternative to Eq. (15). To complete the model, it remains to define priors on $\boldsymbol{\theta}$.

The scope of the method presented in this work is to find the maximum a posteriori (MAP) estimate of $\boldsymbol{\theta}$, minimizing the difference between experimental data and simulated prediction, subject to reasonable priors on the model error. This is an inverse problem and can be formulated in a general way using Bayes's theorem:

$$p(\boldsymbol{\theta}|\boldsymbol{d}) \propto p(\boldsymbol{d}|\boldsymbol{\theta}) p_0(\boldsymbol{\theta}) \tag{18}$$

where $p_0(\boldsymbol{\theta})$ represents available knowledge about $\boldsymbol{\theta}$ in the absence of $\boldsymbol{d}$; $p(\boldsymbol{d}|\boldsymbol{\theta})$ is the likelihood that represents the probability of observing the data given a certain value of $\boldsymbol{\theta}$, modeled with Eq. (17); and $p(\boldsymbol{\theta}|\boldsymbol{d})$ is the posterior probability distribution, which is the updated probability of $\boldsymbol{\theta}$ informed by the data. The posterior is not a single parameter vector but a distribution over the parameter space. Therefore, when a representative realization of control parameters must be chosen, one reasonable choice is the maximum a posteriori estimate of $p(\boldsymbol{\theta}|\boldsymbol{d})$. Since we assumed that the observations are i.i.d., the likelihood function can be written as

$$p(\boldsymbol{d}|\boldsymbol{\theta}) = p(d_1|\boldsymbol{\theta}) \cdot p(d_2|\boldsymbol{\theta}) \cdot \ldots p(d_N|\boldsymbol{\theta})$$

Furthermore, we assume that they are normally distributed with the constant standard deviation σ_{exp} and mean given by $\mathcal{B}(\boldsymbol{\theta}) \coloneqq \mathcal{B}(\boldsymbol{U}(\boldsymbol{\theta}))$ Hence, the likelihood is

$$p(\boldsymbol{d}|\boldsymbol{\theta}) = \left(\frac{1}{\sigma_{\text{exp}}\sqrt{2\pi}}\right)^{N_d} \exp\left\{-\sum_{i=1}^{N_d} \frac{[\mathcal{B}(\boldsymbol{\theta})_i - d_i]^2}{2\sigma_{\text{exp}}^2}\right\} \tag{19}$$

In case of uninformative objective priors, we have that $p(\boldsymbol{\theta}|\boldsymbol{d}) \propto p(\boldsymbol{d}|\boldsymbol{\theta})$ and the MAP estimate can be found by minimizing the negative of the exponent of the likelihood function as

$$\min_{\boldsymbol{\theta}} \hat{\mathcal{J}} = \min_{\boldsymbol{\theta}} \sum_{i=1}^{N_d} \frac{[\mathcal{B}(\boldsymbol{\theta})_i - d_i]^2}{2\sigma_{\text{exp}}^2} \tag{20}$$

If, on the other hand, we choose to specify a prior probability density function for our control parameters $\boldsymbol{\theta}$, and we assume they are independent and normally distributed with mean given by $\theta_{j,\text{prior}}$ for $j = 1, \ldots, N_m$ and standard deviation $\sigma_{j,\theta}$, the MAP can be obtained as

$$\min_{\boldsymbol{\theta}} \mathcal{J} = \min_{\boldsymbol{\theta}} \sum_{i=1}^{N_d} \frac{[\mathcal{B}(\boldsymbol{\theta})_i - d_i]^2}{2\sigma_{\text{exp}}^2} + \sum_{j=1}^{N_m} \frac{(\theta_j - \theta_{j,\text{prior}})^2}{2\sigma_{j,\theta}^2} \tag{21}$$

The second term in Eq. (21) acts as a regularization term that penalizes departures of the parameter vector from its presumed value. In this work, $\boldsymbol{\theta} = [\alpha_\infty, M_\infty, \boldsymbol{\beta}]^\top$, where $\boldsymbol{\beta}$ corrects functional errors in the FANS turbulence model, whereas the optimum α_∞ and M_∞ are the interference-free angle of attack and Mach number. This is a high-dimensional vector with $N_m + 2$ parameters.

III. Results

In this section, the data assimilation methodology presented in Sec. II is used to obtain the wind-tunnel wall-interference corrections for 2-D and 3-D experiments with nonlinear effects. The selected test

cases are the high-Mach-number small angle-of-attack experiment on the RAE 2822 airfoil conducted by Cook et al. in 1979 [37], the low-Mach-number high angle-of-attack experiment on the s809 airfoil by Somers [38], and the high-Mach-number small angle-of-attack experiment on the ONERA M6 wing [39]. While the framework presented in this work can be used with different types of experimental data (e.g., velocity, pressure, skin friction, etc.), we choose to use only surface pressure data because these are one of the most common types of data obtainable from experiments. For the purpose of this work, the data of Cook et al. [37] and Somers [38] are considered to be perfectly 2-D, and thus free of sidewall interference. However, it should be acknowledged that sidewall effects may be present due to the relatively small aspect ratio ($AR < 4$) of the wings used for the experiments.

The initial Mach number and angle of attack for each optimization are set to the values obtained from a conventional correction procedure. Furthermore, the results of the data assimilation methodology using $\boldsymbol{\theta}_\beta = [\alpha_\infty, M_\infty, \boldsymbol{\beta}]^\top$ as the vector of control parameters will be compared with those of a data assimilation using $\boldsymbol{\theta} = [\alpha_\infty, M_\infty]^\top$ in order to show how correcting functional errors in the turbulence model affects the wall-interference corrections.

A. RAE 2822: Case 10

Among all the configurations tested by Cook et al. [37], the one at $M_\infty = 0.75$ and $\alpha_\infty = 3.06$ deg (case 10) presents shock-induced boundary-layer separation, which makes it hard to find adequate wall-interference corrections using linear techniques and has proven challenging to simulate with CFD. A correction to these values was proposed by Rudnik [40], who kept the same Mach number while lowering the angle of attack to 2.80 deg. Rudnik's correction is adopted as the initial condition for α_∞ and M_∞ of the data assimilation methodology. A value of $\sigma_{\text{exp}} = 2.6 \times 10^{-3}$ is selected in accordance with the data in Ref. [37]. A standard deviation of unity is assigned to all the other parameters.

A hybrid O-mesh geometry is used, with the far-field boundary placed 100 chord lengths away from the airfoil to avoid reflections of characteristic waves back into the domain. A no-slip adiabatic boundary condition is imposed on the airfoil while characteristic-based boundary conditions are specified at the far field. A layer of structured cells is wrapped around the airfoil, whereas the rest of the domain is filled with triangular cells. The maximum cell height in the boundary-layer mesh is selected such that $y^+ \approx 1$. The mesh, which has 24,086 points with 287 edges on the airfoil surface, can be seen in Fig. 1.

The convective fluxes are discretized with a second-order Jameson–Schmidt–Turkel scheme [41], and the gradients for the viscous fluxes are computed using a weighted least-squares method. Implicit local time stepping is used to converge the simulation to a steady-state solution, and the linear system is solved using the iterative Generalized Minimal Residual method with a tolerance of $\mathcal{O}(10^{-6})$ on the maximum error.

Figure 2 shows the optimization history for the case with $\boldsymbol{\theta}_\beta$ and $\boldsymbol{\theta}$ (which corresponds to the technique proposed by Ma et al. [14]). Both techniques are capable of reducing the difference between the numerical and experimental pressure coefficients on the airfoil compared to the initial state. Both optimization histories show the same behavior for the first 20 iterations, indicating that the bulk of the improvements is due to changes to the angle of attack and Mach number. However, when $\boldsymbol{\beta}$ is included in the vector of control parameters, an additional reduction of $\hat{\mathcal{J}}$ is observed thanks to small corrections of inadequacies in the turbulence model. This comes at the cost of a higher number of optimization iterations. Indeed, since $\boldsymbol{\theta}_\beta$ is a high-dimensional vector with more than 20,000 control parameters, the optimization algorithm searches in a comparatively high-dimensional space, hence the larger number of optimization iterations compared to the case with $\boldsymbol{\theta}$, which is only a bidimensional vector.

Figure 3 shows the initial c_p distribution for the baseline case (obtained with angle of attack and Mach number proposed by Rudink [40]), the final c_p distributions from the optimizations with $\boldsymbol{\theta}$ and $\boldsymbol{\theta}_\beta$, and the experimental data. The optimized results better capture the shock location but slightly underestimate the magnitude of the pressure peak at the leading edge. In addition, the optimization with $\boldsymbol{\theta}_\beta$ accurately reproduces the pressure distribution after the shock,

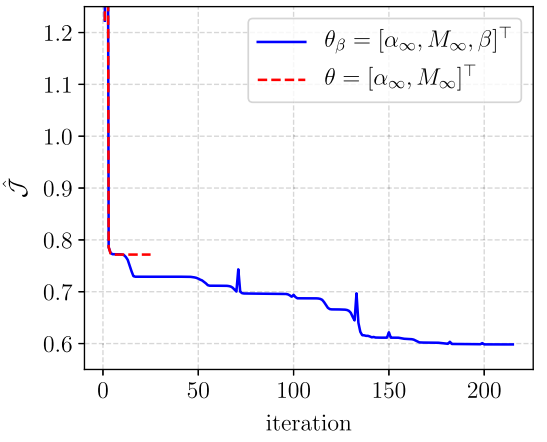

Fig. 2 Optimization histories for the RAE 2822 test case.

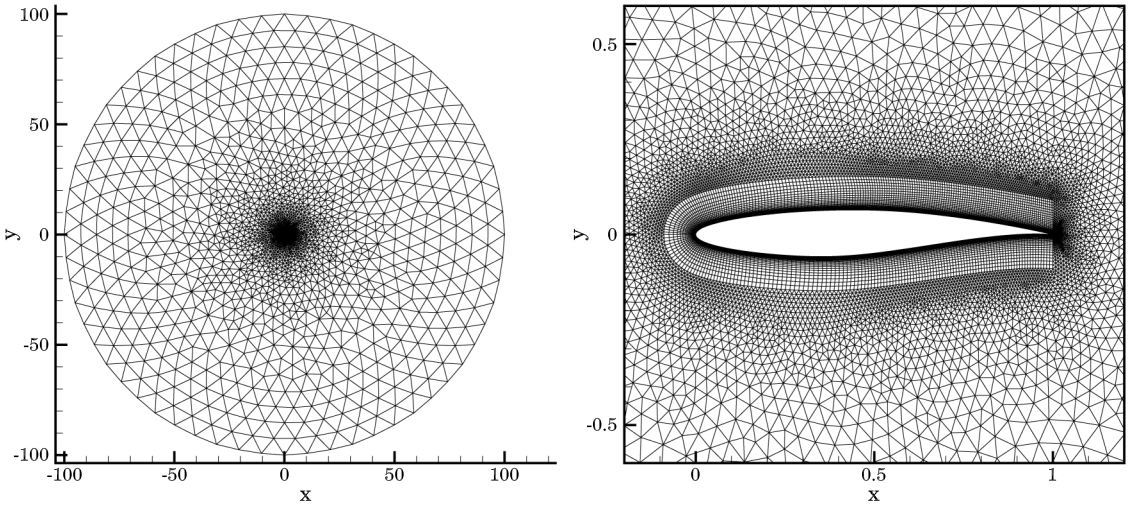

a) The complete computational domain **b) Close-up of the mesh topology in the airfoil region**

Fig. 1 Details of the hybrid computational mesh for the RAE 2822 airfoil.

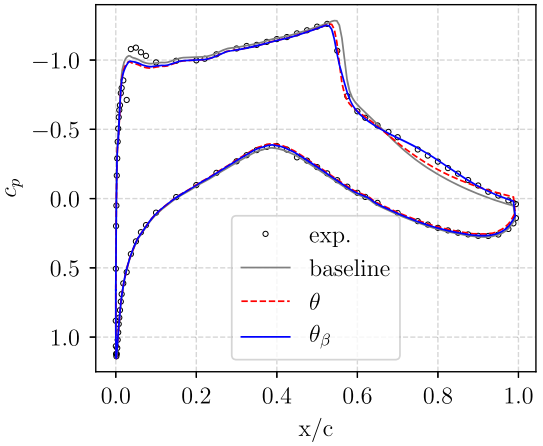

Fig. 3 Comparison of the c_p distribution from the optimizations, the experiment (exp.), and the baseline simulation (obtained by running a turbulent CFD simulation with M_∞ and α_∞ from Ref. [40]).

whereas the optimization with $\boldsymbol{\theta}$ still shows some disagreement due to its inability to correct the errors due to the turbulence model.

Table 1 summarizes some of the results for this test case. We observe that the c_l and c_m predicted by the data assimilation technique proposed in this work are very close to those measured in the experiment. This is not surprising since the lift and the pitching-moment coefficients are closely related to the pressure distribution over the airfoil. The optimization with $\boldsymbol{\theta}_\beta$ as the vector of control parameters reduces the value of the initial $\hat{\mathcal{J}}$ by 50%. On the other hand, the optimization with $\boldsymbol{\theta}$ as vector of control parameters reduces the value of $\hat{\mathcal{J}}$ by 35%. The optimum angle of attack and Mach number from both data assimilation techniques are higher than the baseline case, but they substantially differ from each other, especially in the proposed angle-of-attack correction, thus showing that including $\boldsymbol{\beta}$ in the vector of control parameters has a profound effect on the wall-interference corrections.

Finally, by looking at the boundary-layer comparison of Fig. 4, one can observe that it is easy for the CFD solver to reproduce the boundary-layer shape before the shock location but much harder to do so consistently downstream of it. Indeed, the boundary-layer shape from the optimizations agrees well with the experimental one at $x/c = 0.75$ but not at $x/c = 0.9$, and vice versa for the baseline results. This is an indication that there might not be an equivalent free-air condition to the in-tunnel one, and thus the results are uncorrectable, possibly due to the presence of sidewall effects. It is also likely that the experimental pressure coefficient is not sufficiently informative to exactly reconstruct unobserved quantities (like the velocity field) all over the computational domain. Alternatively, it could be that the flow physics behind the shock and close to the wall cannot be completely reproduced by eddy viscosity models, even when corrected with the methodology proposed in this work. To increase the quality of the reconstruction of the velocity field, one could also incorporate the experimental data for the boundary layers in the objective function and, in general, all available experimental data. This would constrain the optimizer to agree as best as it can with all the different sources of experimental data used in the objective function, thus making it less likely to observe large deviations like the one in Fig. 4d.

Table 1 Comparison of results from proposed methodology with different wind-tunnel wall-interference correction techniques used as benchmark for the RAE 2822 case

	$\hat{\mathcal{J}}$	α_∞, deg	M_∞	c_l	c_m
Experimental data	— —	3.19	0.750	0.743	−0.1060
Baseline	1.223	2.80	0.750	0.747	−0.1007
$\boldsymbol{\theta}$	0.7716	3.00	0.759	0.720	−0.0997
$\boldsymbol{\theta}_\beta$	0.5983	2.90	0.758	0.736	−0.1069

B. S809 Airfoil

The S809 airfoil is commonly used for the design of the blades of horizontal axis wind turbines and was chosen by Singh and Duraisamy [16] and Singh et al. [42] as the test case for their field-inversion machine-learning (FIML) framework, from which the wall-interference correction methodology presented in this paper is inspired. Experimental data at $Re_c = 2 \times 10^6$, $M_\infty = 0.2$, and at a variety of angles of attack are available from the study of Somers [38]. In our case, we perform the inversion at the highest angle of attack of the database (i.e., $\alpha_\infty = 14.24$ deg) for which a large region of turbulent separation due to an adverse pressure gradient is present. Note that this value for the angle of attack was obtained using a linear correction technique and is used as initial α_∞ for the optimization. Figure 5 shows the computational mesh used for this test case, which is the same structured C grid with approximately 5.5×10^4 points and $y^+ \approx 1$ as in the work of Singh and Duraisamy [16]. Similar boundary conditions as in Sec. III.A were adopted. The pressure coefficient from the experiment of Somers [38] is chosen as training data for the objective function and $\sigma_{\text{exp}} = 0.02$. Because extracting the data is prone to errors in proximity of regions with high gradients, only the suction-side pressure data in the range $0.05 < x/c < 0.8$ were used. The same spatial and time discretizations, linear solver, and optimization algorithm as in Sec. III.A were used. Since compressibility effects are limited, the Mach number is excluded from the control parameters used for the correction procedures such that $\boldsymbol{\theta} = \alpha_\infty$ and $\boldsymbol{\theta}_\beta = [\alpha_\infty, \boldsymbol{\beta}]^\top$.

From the optimization history in Fig. 6, one can observe that only correcting the angle of attack has a minimal impact on the error between experiments and simulations. The proposed correction to the angle of attack may very well be right; but, there is no way to assess this since the value of $\hat{\mathcal{J}}$ (which gives an indication of the accuracy of the corrections) remains high because errors due to the turbulence model are affecting the simulation results: hence the importance of having the corrective term $\boldsymbol{\beta}$ among the control parameters. It is evident that the high $\hat{\mathcal{J}}$ is due to turbulence-modeling error; by correcting this error, an estimate of the accuracy of the corrections can thus be obtained.

Figure 7 shows the baseline and assimilated pressure and skin-friction coefficients over the airfoil. The SST model overpredicts the pressure on the suction side and predicts the location of the separation point more downstream than in the experiments. As already observed, correcting only the angle of attack does not change the pressure distribution, whereas correcting the functional errors in the turbulence model produces an almost-perfect match with the experimental data.

The turbulent viscosities μ_{turb} for the baseline and corrected results is showed in Fig. 8. A significant increase of its value in the wake region is produced by the correction procedure proposed in this paper, as shown in Fig. 8c, which indicates the presence of a stronger turbulent flow enhancing the mixing in that region. These considerations can be useful during the development phase of a product since they complement the sparse information of the experimental results with full-field data corresponding to the numerical simulation that best match the experiments.

Table 2 summarizes the results for this test case. The methodology proposed in this work is compared with the results from the baseline case (i.e., the initial condition of the optimization with the in-tunnel angle of attack and Mach number, as well as $\boldsymbol{\beta}$ equal to unity) and a benchmark case, which only optimizes the angle of attack. Although the corrections to the angle of attack are small, the agreement with the experimental lift coefficient is significantly improved by the methodology proposed in this work, whereas that with the pitching-moment coefficient is slightly degraded. Hence, we can conclude that, for this test case, no significant wall interference is present and a linear correction procedure is appropriate. However, the data assimilation methodology not only finds the corrected angle of attack but also corrects the numerical model so that its full-field results can be used to reliably analyze the flow dynamics of the test object. Furthermore, the value of $\hat{\mathcal{J}}$ can be used to estimate the reliability of

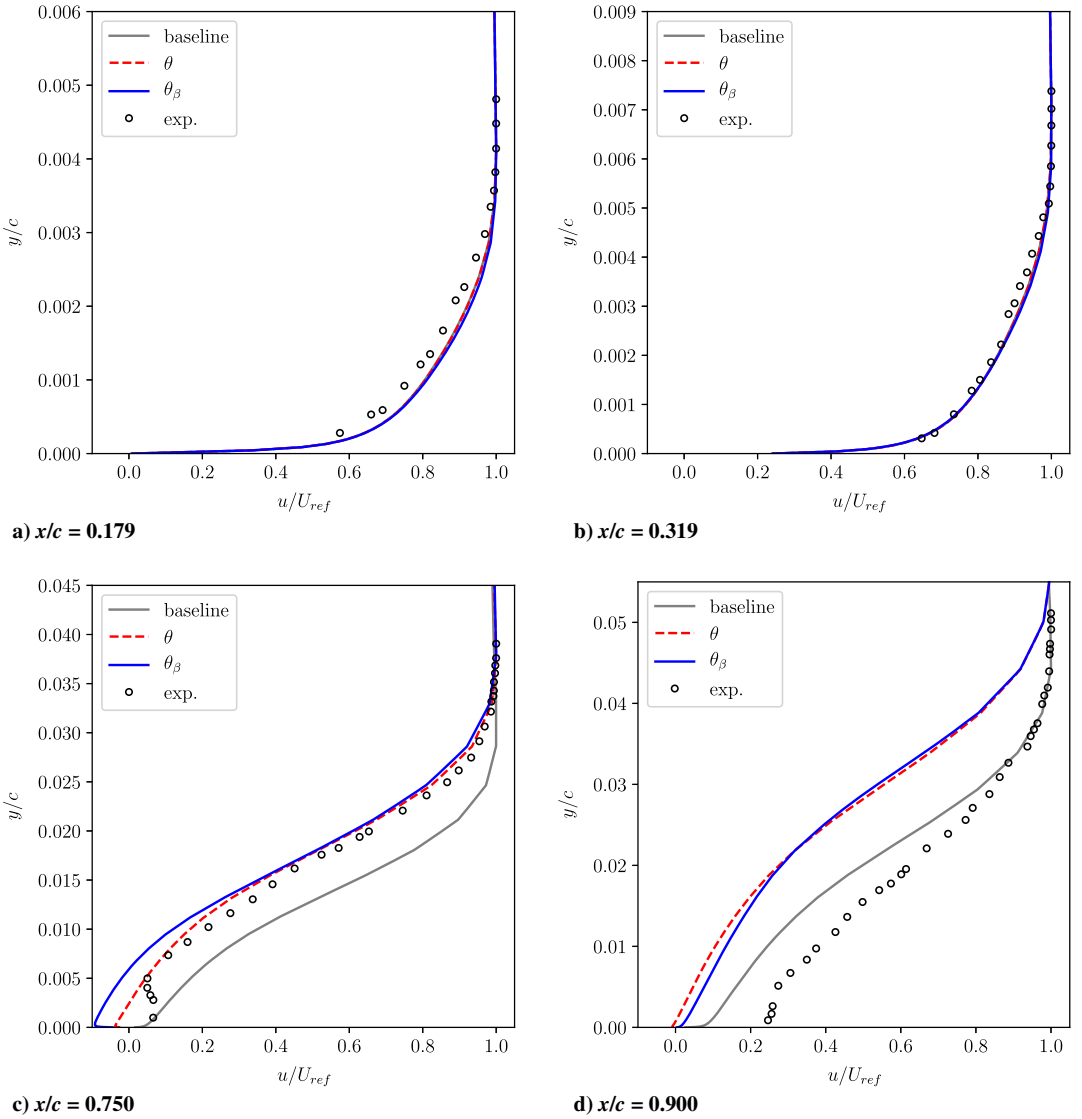

a) *x/c* = 0.179 b) *x/c* = 0.319

c) *x/c* = 0.750 d) *x/c* = 0.900

Fig. 4 Comparison of boundary layers at different x/c locations on the upper surface of the RAE 2822 airfoil.

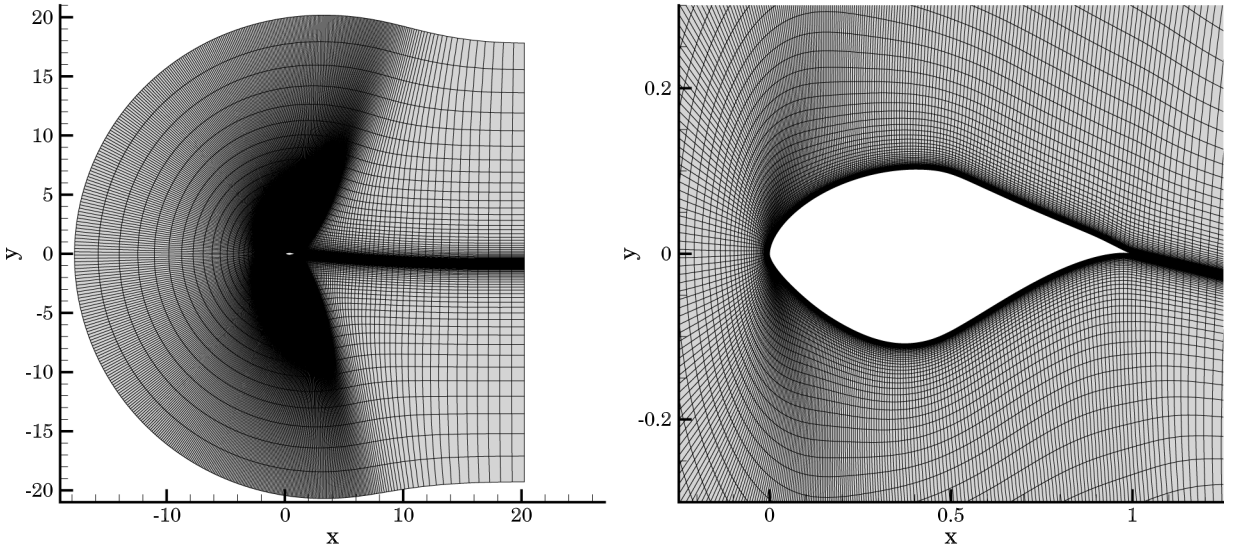

a) The complete computational domain for the s809 test case b) Close-up of the mesh topology in the airfoil region

Fig. 5 Details of the structured computational mesh.

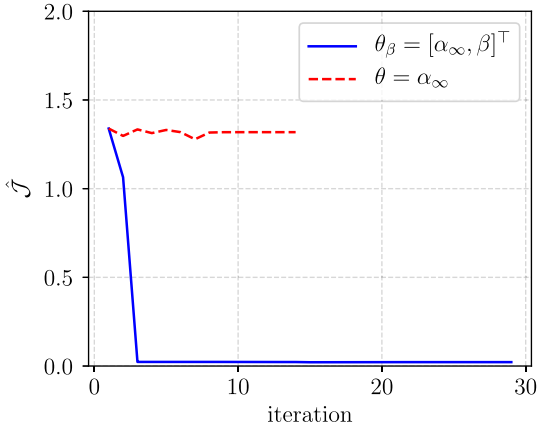

Fig. 6 Optimization histories for the s809 test case.

the proposed corrections based on the agreement between experimental and numerical data.

C. ONERA M6 Wing

The ONERA M6 wing is a widely used test case for the validation of numerical models thanks to the availability of experimental data for a variety of flow conditions [39]. In this work, the Reynolds number based on the mean aerodynamic chord is 11.72×10^6, $M_\infty = 0.8395$, and $\alpha_\infty = 3.06$ deg. For these flow conditions, the leading-edge acceleration leads to supersonic flow that is terminated by a shock wave. From there, the flow is reaccelerated to supersonic conditions again until a second shock is formed. This creates a lambda-shaped low-pressure area between the two shocks. A structured semispherical mesh is used for the simulations, with the flat side being the plane of symmetry of the domain and of the wing. Characteristic boundary conditions are specified at the far field, and the no-slip condition is used for the wing surface. In total, the mesh has 6.6×10^5 points and a y^+ of approximately unity. Experimental pressure coefficients at spanwise locations $y/b = 0.2, 0.44, 0.65, 0.8, 0.9, 0.95$, and 0.99 are used in the error function $\hat{\mathcal{J}}$; and $\sigma_{\text{exp}} = 0.02$ is used. The same spatial and time discretizations, linear solver, and optimization algorithm as in Sec. III.A are used. It is worth noting that the half-wing model was attached to a rotating plate in the experiment, whereas a symmetry boundary condition is employed at $y = 0$ in the numerical domain; and this may alter the flow physics at the wing root. Nonetheless, we attribute these differences to wall-interference effects and focus our analysis on the feasibility of using the proposed methodology for correcting wind-tunnel wall interference rather than exactly reproducing the flow physics.

Table 2 Comparison of results from proposed methodology with different baseline and benchmark results for the s809 case

	$\hat{\mathcal{J}}$	α_∞, deg	M_∞	c_l	c_m
Experimental data	— —	14.24	0.2	1.083	−0.0451
Baseline	1.339	14.24	0.2	1.240	−0.0450
$\boldsymbol{\theta}$	1.331	14.21	0.2	1.239	−0.0450
$\boldsymbol{\theta}_\beta$	0.022	14.23	0.2	1.105	−0.0440

The optimization history of Fig. 9 shows the typical behavior observed so far, whereby the proposed methodology reduces the discrepancy between the experimental and numerical data significantly over the baseline and benchmark cases. Compared to the 2-D cases, $\hat{\mathcal{J}}$ is orders of magnitude higher since there are many more experimental data points contributing to its value. As a consequence, judging the accuracy of the corrections based on the value of $\hat{\mathcal{J}}$ is

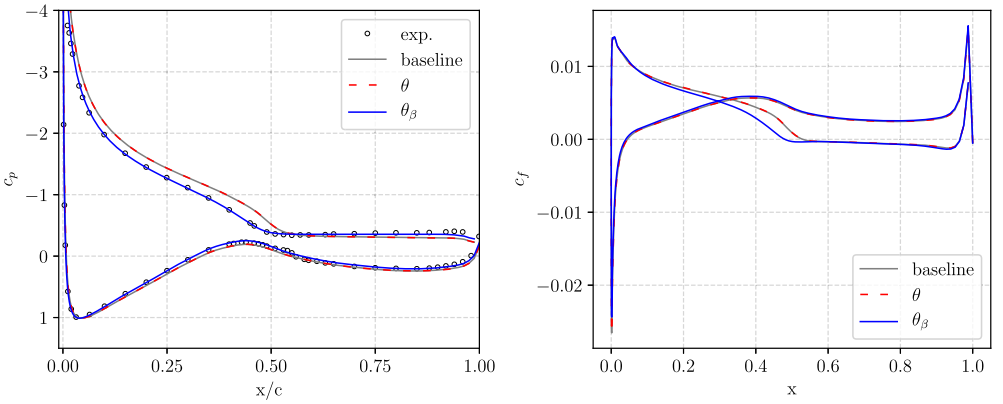

a) Pressure coefficient **b) Skin-friction coefficient**

Fig. 7 Comparison of the c_p and c_f distributions from the optimizations, the experimental data, and the baseline simulation for the s809 test case.

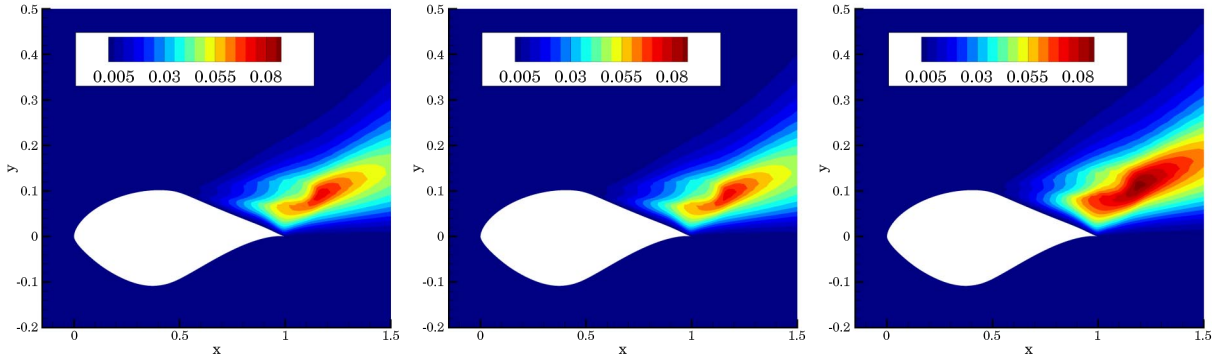

a) Initial condition (baseline) **b) $\theta = \alpha_\infty$** **c) $\theta_\beta = [\alpha_\infty, \beta]^\top$**

Fig. 8 Comparison turbulent viscosity μ_{turb} for the s809 test case.

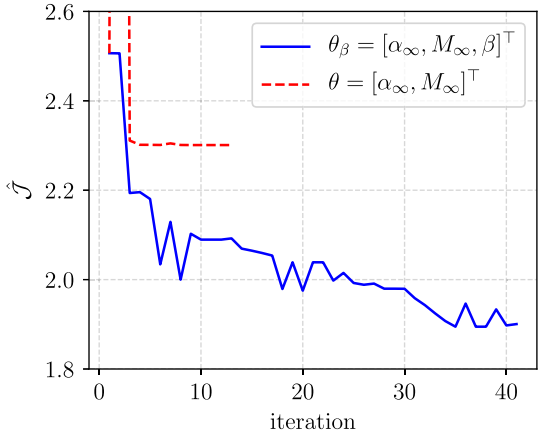

Fig. 9 Optimization histories for the ONERA M6 test case.

dependent on the number of experimental observations. To overcome this limitation, one can simply look at the mean squared error $\hat{\mathcal{J}}/N_m$.

The methodology proposed in this work improves the agreement with the experimental pressure distributions compared to the baseline and benchmark cases as shown in Fig. 10: especially at $y/b = 0.2$, where it is able to correctly predict the location of the second shock. However, there are still differences at $y/b = 0.65$ and at $y/b = 0.8$, where the strength of the first shock is not fully captured. This could be due to discretization errors, but the study of Mayeur et al. [43] shows that this phenomenon is present even for meshes of 10 million points. This suggests that the underestimation of the shock strength is purely due to turbulence-model inadequacies. While our correction procedure is able to change the balance of terms in the functional form of the model, it is still forced to operate within the boundaries imposed by the Boussinesq hypothesis. Hence, more general corrective models like the one presented by Belligoli et al. [21] should be examined for solving these issues.

By looking at the turbulent viscosity fields of Fig. 11, we observe no significant differences between the initial solution and the optimum solution found by the optimization with $\boldsymbol{\theta}$ as a vector of control parameters. On the other hand, when $\boldsymbol{\theta}_\beta$ is used, a significant change to the μ_{turb} field close to the wing root is observed. This looks unphysical, and it is probably due to different boundary conditions between the experiment and the simulations. Indeed, the simulations employ a symmetry boundary condition at $y = 0$, whereas a wall was present at the same location in the experiment. This is an indication of the failure of half-model testing to reproduce the properties of a symmetry plane.

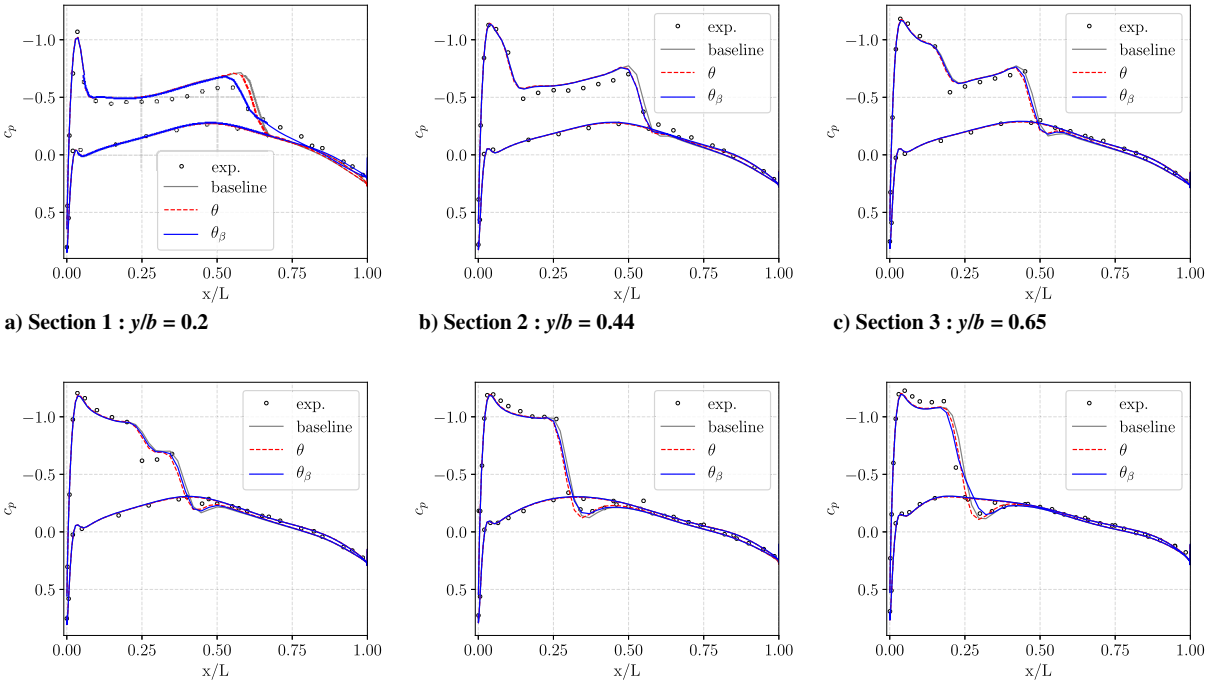

a) Section 1 : *y/b* = 0.2 **b) Section 2 : *y/b* = 0.44** **c) Section 3 : *y/b* = 0.65**

d) Section 4 : *y/b* = 0.8 **e) Section 5 : *y/b* = 0.9** **f) Section 6 : *y/b* = 0.95**

Fig. 10 Comparison of c_p distributions at six of the seven locations where experimental data are available.

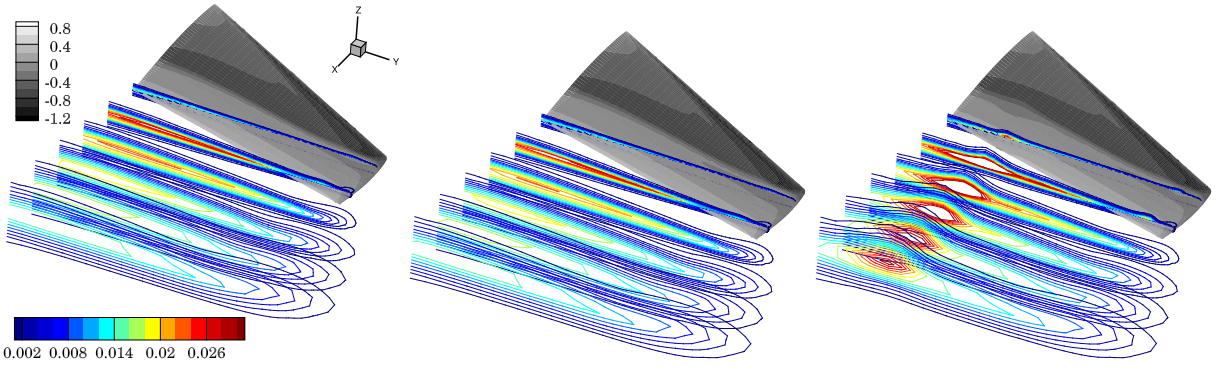

a) Baseline **b) $\theta = \{\boldsymbol{\alpha_\infty}, \boldsymbol{M_\infty}\}$** **c) $\boldsymbol{\theta_\beta} = [\alpha_\infty, M_\infty, \beta]^\top$**

Fig. 11 Comparison of c_p contours on the wing and μ_{turb} isosurfaces in the wake for the ONERA M6 test case.

Table 3 Comparison of results from proposed methodology with different baseline and benchmark results for the ONERA M6 case

	$\hat{\mathcal{J}}$	α_∞, deg	M_∞
Experimental data	— —	3.060	0.8395
Baseline	2.507	3.060	0.8395
$\boldsymbol{\theta}$	2.301	3.026	0.8367
$\boldsymbol{\theta}_\beta$	1.888	3.055	0.8389

To complete the analysis, we report the values of $\hat{\mathcal{J}}$, α_∞, and M_∞ in Table 3, where we can see how only small changes to the angle of attack and Mach number are obtained after using the framework proposed in this work. Nonetheless, together with the corrections to the functional errors in the turbulence model operated by $\boldsymbol{\beta}$, they contribute to reduce the least-square error $\hat{\mathcal{J}}$ between experimental data and corresponding numerical data by about 25%.

IV. Conclusions

The wall-interference correction methodology presented in this work was developed for the nonlinear flow regime. For this, the compressible FANS equations and a turbulence model for capturing viscous phenomena are used. A gradient-based optimization problem must be solved to obtain the optimum corrections. The progress in computer hardware and numerical algorithms made it possible to carry out this process within a few days at the most (depending on the available computational resources, the number of mesh points, and the size of the vector of control parameters). However, wind-tunnel operators usually prefer to have online corrections to immediately analyze whether interference is small. In this view, the nonlinear correction technique of this work can be used as an offline tool to obtain more accurate wall-interference corrections, as well as to augment the experimental data with full-field information of the case at hand.

The optimum solution found by the optimization gives the best possible agreement with the experimental data used in the objective function $\mathcal{J}$, given the initial conditions; and the mathematical model used. However, the solution of this ill-posed inverse problem is nonunique. The regularization term in the objective function makes sure that the optimum solution lies in a neighborhood of the initial state by penalizing strong departures of the control variables from their initial values.

One of the fundamental assumptions of the data assimilation methodology is that the experimental data are the ground truth and that there exists a free-air condition that gives the same in-tunnel results. Traditionally, this assumption was not always used and linear techniques not only corrected the flow conditions but also the force coefficients. In the current methodology, this choice is left to the user: based on their knowledge, they can either use the experimental data as ground truth and use the value of the mean squared error $\hat{\mathcal{J}}/N_m$ to estimate the accuracy of the corrections, or thye can decide to accept the numerically obtained pressure distribution in place of the experimental one.

For simplicity, only experimental pressure coefficients were used on the wing surface for the test cases of Sec. III. However, any type of physical quantity obtainable from an experiment can be inserted in the objective function and multiple physical quantities can coexist (e.g., velocity and pressure). Hence, one can make use of all the experimental data at their disposal for finding the optimum value of the corrections. Obviously, the more data there are available, the more information there is available for the optimizer to find the true optimum; but, the data assimilation methodology presented in this work can function with a very limited number of data points.

Finally, it is worth remembering that this technique does not require representation and modeling of the wind-tunnel walls since the optimization is directly carried out in free air. This removes a great burden from the correction procedure, namely, that of finding an accurate model for the ventilated boundary condition and that of meshing the entire geometry of the wind-tunnel walls to accurately represent the flow through the ventilated surfaces. However, the data assimilation technique can also be used to reconstruct the in-tunnel flowfield by including the wind-tunnel wall geometry in the CFD mesh.

The methodology proposed in this work is more time consuming than linear correction techniques and can only be carried out offline. Additionally, the correction to the turbulence model is limited in scope because it must comply with the Boussinesq hypothesis and it can only address errors within its functional form. Future work should focus on testing more general corrections to the errors introduced by the modeling of turbulence, as well as on the combination of different types of experimental data (e.g., velocity and pressure) into the same objective function. In this regard, other choices than constant diagonal covariance matrices are possible and can be used to cope with experimental data with nonuniform uncertainty.

References

[1] Melanson, M., Chang, M., and Baker, W., II, "Wind Tunnel Testing's Future: A Vision of the Next Generation of Wind Tunnel Test Requirements and Facilities," *48th AIAA Aerospace Sciences Meeting Including the New Horizons Forum and Aerospace Exposition*, AIAA Paper 2010-0142, 2010. https://doi.org/10.2514/6.2010-142

[2] Ewald, B., "Wind Tunnel Wall Correction," Advisory Group for Aerospace Research and Development TR AGARD-AG-336, Neuilly-Sur-Seine, France, 1998.

[3] Davis, T. W., "Review of Transonic Wall Interference Corrections and Considerations for Development," *AIAA Aviation 2019 Forum*, AIAA Paper 2019-3094, 2019. https://doi.org/10.2514/6.2019-3094

[4] Rueger, M., and Crites, R., "Wind Tunnel Boundary Interference Prediction and Correction," *30th Aerospace Sciences Meeting and Exhibit*, AIAA Paper 1992-0036, 1992. https://doi.org/10.2514/6.1992-36

[5] Martin, F., Jr., Sickles, W., and Stanley, S., "Transonic Wind Tunnel Wall Interference Analysis for the Space Shuttle Launch Vehicle," *31st Aerospace Sciences Meeting*, AIAA Paper 1993-0420, 1993. https://doi.org/10.2514/6.1993-420

[6] Hantrais-Gervois, J.-L., Mouton, S., and Piat, J.-F., "A Methodology to Derive Wind Tunnel Wall Corrections from RANS Simulations," *47th AAAF International Symposium of Applied Aerodynamics. Wind Tunnel and Computation: A Joint Strategy for Flow Prediction*, Paris, France, March 2012.

[7] Nambu, T., Hashimoto, A., Aoyama, T., and Sato, T., "Numerical Analysis of the ONERA-M6 Wing with Wind Tunnel Wall Interference," *Transactions of the Japan Society for Aeronautical and Space Sciences*, Vol. 58, No. 1, 2015, pp. 7–14.

[8] Nambu, T., Hashimoto, A., Ueno, M., Murakami, K., and Sato, T., "Evaluation of Wall-Interference Correction Method Using Numerical Analysis and Porous Wall Model," *Journal of Aircraft*, Vol. 52, No. 1, 2015, pp. 226–234. https://doi.org/10.2514/1.C032675

[9] Hashimoto, A., Aoyama, T., Kohzai, M., and Yamamoto, K., "Transonic Wind Tunnel Simulation with Porous Wall and Support Devices," *27th AIAA Aerodynamic Measurement Technology and Ground Testing Conference*, AIAA Paper 2010-4201, 2010. https://doi.org/10.2514/6.2010-4201

[10] Krynytzky, A., Fleming, M., Sommerfield, D., and Li, P., "Computational Modeling of a Slotted Wall Test Section," *28th Aerodynamic Measurement Technology, Ground Testing, and Flight Testing Conference Including the Aerospace T&E Days Forum*, AIAA Paper 2012-2863, 2012. https://doi.org/10.2514/6.2012-2863

[11] Xiao, H., and Cinnella, P., "Quantification of Model Uncertainty in RANS Simulations: A Review," *Progress in Aerospace Sciences*, Vol. 108, July 2019, pp. 1–31. https://doi.org/10.1016/j.paerosci.2018.10.001

[12] Duraisamy, K., Iaccarino, G., and Xiao, H., "Turbulence Modeling in the Age of Data," *Annual Review of Fluid Mechanics*, Vol. 51, Jan. 2019, pp. 357–377. https://doi.org/10.1146/annurev-fluid-010518-040547

[13] Murman, E. M., "A Correction Method for Transonic Wind Tunnel Wall Interference," *12th Fluid and Plasma Dynamics Conference*, AIAA Paper 1979-1533, 1979. https://doi.org/10.2514/6.1979-1533

[14] Ma, B., Wang, G., Ye, Z., and Xu, L., "A Numerical Method for Transonic Wind Tunnel Wall Interference Correction in Airfoil Testing," *34th AIAA Applied Aerodynamics Conference*, AIAA Paper 2016-3575, 2016.
https://doi.org/10.2514/6.2016-3575

[15] Kato, H., Yoshizawa, A., Ueno, G., and Obayashi, S., "A Data Assimilation Methodology for Reconstructing Turbulent Flows Around Aircraft," *Journal of Computational Physics*, Vol. 283, Feb. 2015, pp. 559–581.
https://doi.org/10.1016/j.jcp.2014.12.013

[16] Singh, A. P., and Duraisamy, K., "Using Field Inversion to Quantify Functional Errors in Turbulence Closures," *Physics of Fluids*, Vol. 28, No. 4, 2016, Paper 045110.
https://doi.org/10.1063/1.4947045

[17] Duraisamy, K., Zhang, Z. J., and Singh, A. P., "New Approaches in Turbulence and Transition Modeling Using Data-Driven Techniques," *53rd AIAA Aerospace Sciences Meeting*, AIAA Paper 2015-1284, 2015.
https://doi.org/10.2514/6.2015-1284

[18] Parish, E. J., and Duraisamy, K., "A Paradigm for Data-Driven Predictive Modeling Using Field Inversion and Machine Learning," *Journal of Computational Physics*, Vol. 305, Jan. 2016, pp. 758–774.
https://doi.org/10.1016/j.jcp.2015.11.012

[19] Singh, A. P., Duraisamy, K., and Zhang, Z. J., "Augmentation of Turbulence Models Using Field Inversion and Machine Learning," *55th AIAA Aerospace Sciences Meeting*, AIAA Paper 2017-0993, 2017.
https://doi.org/10.2514/6.2017-0993

[20] Belligoli, Z., Dwight, R., and Eitelberg, G., "Assessment of a Data Assimilation Technique for Wind Tunnel Wall Interference Corrections," *AIAA SciTech 2019 Forum*, AIAA Paper 2019-0939, 2019.
https://doi.org/10.2514/6.2019-0939

[21] Belligoli, Z., Dwight, R., and Eitelberg, G., "RANS Data Assimilation Techniques for Wind-Tunnel Wall Interference Corrections," *AIAA Aviation 2019 Forum*, AIAA Paper 2019-2976, 2019.
https://doi.org/10.2514/6.2019-2976

[22] Giles, M. B., and Pierce, N. A., "An Introduction to the Adjoint Approach to Design," *Flow, Turbulence and Combustion*, Vol. 65, Nos. 3–4, 2000, pp. 393–415.
https://doi.org/10.1023/A:1011430410075

[23] Pironneau, O., "On Optimum Design in Fluid Mechanics," *Journal of Fluid Mechanics*, Vol. 64, No. 1, 1974, pp. 97–110.
https://doi.org/10.1017/S0022112074002023

[24] Dwight, R. P., and Brezillon, J., "Effect of Approximations of the Discrete Adjoint on Gradient-Based Optimization," *AIAA Journal*, Vol. 44, No. 12, 2006, pp. 3022–3031.
https://doi.org/10.2514/1.21744

[25] Peter, J. E., and Dwight, R. P., "Numerical Sensitivity Analysis for Aerodynamic Optimization: A Survey of Approaches," *Computers and Fluids*, Vol. 39, No. 3, 2010, pp. 373–391.
https://doi.org/10.1016/j.compfluid.2009.09.013

[26] Albring, T. A., Sagebaum, M., and Gauger, N. R., "Development of a Consistent Discrete Adjoint Solver in an Evolving Aerodynamic Design Framework," *16th AIAA/ISSMO Multidisciplinary Analysis and Optimization Conference*, AIAA Paper 2015-3240, 2015.
https://doi.org/10.2514/6.2015-3240

[27] Albring, T. A., Sagebaum, M., and Gauger, N. R., "Efficient Aerodynamic Design Using the Discrete Adjoint Method in SU2," *17th AIAA/ISSMO Multidisciplinary Analysis and Optimization Conference*, AIAA Paper 2016-3518, 2016.
https://doi.org/10.2514/6.2016-3518

[28] Economon, T. D., Palacios, F., Copeland, S. R., Lukaczyk, T. W., and Alonso, J. J., "SU2: An Open-Source Suite for Multiphysics Simulation and Design," *AIAA Journal*, Vol. 54, No. 3, 2016, pp. 828–846.
https://doi.org/10.2514/1.j053813

[29] Vitale, S., Gori, G., Pini, M., Guardone, A., Economon, T. D., Palacios, F., Alonso, J. J., and Colonna, P., "Extension of the SU2 Open Source Cfd code to the Simulation of Turbulent Flows of Fluids Modelled with Complex Thermophysical Laws," *22nd AIAA Computational Fluid Dynamics Conference*, AIAA Paper 2015-2760, 2015.
https://doi.org/10.2514/6.2015-2760

[30] Liu, D. C., and Nocedal, J., "On the Limited Memory BFGS Method for Large Scale Optimization," *Mathematical Programming*, Vol. 45, Nos. 1–3, 1989, pp. 503–528.
https://doi.org/10.1007/BF01589116

[31] Gatski, T. B., and Bonnet, J.-P., *Compressibility, Turbulence and High Speed Flow*, Academic Press, New York, 2013, pp. 54–56.

[32] Menter, F. R., "Two-Equation Eddy-Viscosity Turbulence Models for Engineering Applications," *AIAA Journal*, Vol. 32, No. 8, 1994, pp. 1598–1605.
https://doi.org/10.2514/3.12149

[33] Kennedy, M. C., and O'Hagan, A., "Bayesian Calibration of Computer Models," *Journal of the Royal Statistical Society: Series B (Statistical Methodology)*, Vol. 63, No. 3, 2001, pp. 425–464.
https://doi.org/10.1111/1467-9868.00294

[34] Edeling, W., Cinnella, P., and Dwight, R. P., "Predictive RANS Simulations via Bayesian Model-Scenario Averaging," *Journal of Computational Physics*, Vol. 275, Oct. 2014, pp. 65–91.
https://doi.org/10.1016/j.jcp.2014.06.052

[35] Cheung, S. H., Oliver, T. A., Prudencio, E. E., Prudhomme, S., and Moser, R. D., "Bayesian Uncertainty Analysis with Applications to Turbulence Modeling," *Reliability Engineering and System Safety*, Vol. 96, No. 9, 2011, pp. 1137–1149.
https://doi.org/10.1016/j.ress.2010.09.013

[36] Edeling, W., Cinnella, P., Dwight, R. P., and Bijl, H., "Bayesian Estimates of Parameter Variability in the k-ε Turbulence Model," *Journal of Computational Physics*, Vol. 258, Feb. 2014, pp. 73–94.
https://doi.org/doi.org/10.1016/j.jcp.2013.10.027

[37] Cook, P., Firmin, M., and McDonald, M., "Aerofoil RAE 2822: Pressure Distributions, and Boundary Layer and Wake Measurements," AGARD-AR-138, 1977, pp. A6-1–A6-77.

[38] Somers, D. M., "Design and Experimental Results for the S809 Airfoil," National Renewable Energy Lab. TR NREL/SR-440-6918, Golden, CO, 1997.

[39] Schmitt, V., "Pressure Distributions on the ONERA M6-wing at Transonic Mach Numbers, Experimental Data Base for Computer Program Assessment," AGARD Rept. AR-138, Neuilly-Sur-Seine, France, 1979.

[40] Rudnik, R., "Untersuchung der Leistungsfähigkeit von Zweigleichungs-Turbulenzmodellen bei Profilumströmungen," Dissertation, Forschungsbericht-Deutsches Zentrum Fur Luft Und Raumfahrt, DLR-Forschungsbericht, 1997, pp. 97–49.

[41] Jameson, A., Schmidt, W., and Turkel, E., "Numerical Solution of the Euler Equations by Finite Volume Methods Using Runge Kutta Time Stepping Schemes," *14th Fluid and Plasma Dynamics Conference*, AIAA Paper 1981-1259, 1981.
https://doi.org/10.2514/6.1981-1259

[42] Singh, A. P., Medida, S., and Duraisamy, K., "Machine-Learning-Augmented Predictive Modeling of Turbulent Separated Flows over Airfoils," *AIAA Journal*, Vol. 55, No. 7, 2017, pp. 2215–2227.
https://doi.org/10.2514/1.J055595

[43] Mayeur, J., Dumont, A., Destarac, D., and Gleize, V., "RANS Simulations on TMR Test Cases and M6 Wing with the Onera elsA Flow Solver," AIAA Paper 2015-1745, 2015.
https://doi.org/10.2514/6.2015-1745

A. R. Jones
Associate Editor